Available online at www.sciencedirect.com
ScienceDirect
Energy Procedia 1 (2009) 3351–3358
Energy Procedia
www.elsevier.com/locate/procedia

GHGT-9

Experimental percolation of supercritical CO_2 through a caprock

Matthieu Angeli, Magnus Soldal, Elin Skurtveit and Eyvind Aker

Norges Geotekniske Institutt, Sognsveien 72, 0806 Oslo, Norway

Abstract

Leakage of CO_2 into the atmosphere is the most crucial concern for geological storage of anthropogenic CO_2. Leakage routes could develop through existing wells and pipelines, but also by natural migration of CO_2 rich pore-fluid through the caprock and in fault zones. Therefore, a thorough geological characterization of the prospective formation identifying seal capacity, integrity and possible migration pathways must be performed prior to injection of CO_2. A caprock is a low permeable confining layer trapping CO_2 stored in a reservoir rock. Although the caprock acts as a seal, its lower boundary will be in contact with CO_2 saturated pore water or even pure CO_2. Chemical interaction between the pore fluid and the caprock may change its material properties.

The aim of this study is to increase our understanding of the interaction between CO_2 and caprock, focusing on the microstructural properties of the rock. A flow through cell is used to flood a shale core (40 mm long and 38 mm diameter) with supercritical CO_2 at a temperature of 35° C and at pressures above 7.5 MPa. A pressure gradient is applied across the sample to obtain a breakthrough of CO_2 in the core. During flooding both axial and radial strain of the core are measured together with the acoustic velocities in the axial direction. The measurements are performed both for the brine saturated core and at various stages during flooding with CO_2. The experimental results suggest flow of CO_2 along defined pathways within the shale. These pathways are likely to be controlled by the increasing pore pressure at the bottom of the sample which allows reopening of the cracks in the lower part of the sample, allowing CO_2 to enter the shale. Flow of CO_2 into the cracks in the lower part of the sample is followed by percolation of CO_2 in the upper part of the sample where the effective pressure is higher and crack re-opening is less likely to occur.

Keywords: CO_2 storage; caprock; breakthrough

1. Introduction

Leakage of CO_2 into the atmosphere is the most crucial concern for geological storage of anthropogenic CO_2. Leakage routes could develop through existing wells and pipelines but also by natural migration of CO_2 rich pore-fluid through the caprock and in fault zones. Apart from events like seismically induced seal rupture or tectonic strains, the sealing capacity of a caprock is controlled by the capillary entry pressure, permeability and molecular diffusion [1]. Therefore, a thorough geological characterization of the prospective formation identifying seal capacity, integrity and possible migration pathways must be performed prior to injection of CO_2.

Laboratory methods for characterization of sealing capacity of caprock for CO_2 storage is similar to methods

doi:10.1016/j.egypro.2009.02.123

used for estimating sealing capacity for hydrocarbons. Prior studies focusing on CO_2 storage include measurements of capillary entry and gas breakthrough pressure [2, 3], diffusion [4], CO_2/water interfacial tension [5] and relative permeability of brine and CO_2 [6]. Migration of CO_2 into the caprock may trigger geochemical reactions affecting crucial parameters such as porosity and permeability [7] or dissolve organic matter [8] which is found to have a minor affect the slow Darcy flow in the sealing formation. Pore pressure changes due to injection of CO_2 depends on the volume and permeability of the storage reservoir, and may generate both shear and tensile failure above the injection site under specific initial stress conditions [9].

In this study direct measurement of CO_2 breakthrough pressure is performed together with monitoring of flow, strain and acoustic velocity in order to assess the geomechanical changes in the caprock during CO_2 injection.

2. Materials

The shale material (fig. 1) used in the experiment comes from the Troll East field. The Troll field is located approximately 65 km off the west coast of Norway in the northern part of the North Sea. The seal peel, from which the sample is taken, belongs to the Upper Jurassic Draupne Formation and was drilled 1360 meters beneath sea level (water depth around 350 m). It is the third caprock above the Johansen formation, a porous sandstone formation in North-East North Sea and a possible CO_2 storage site off shore the west coast of Norway. Since 1998, the shale material has been kept in a cooling room under moderate axial load. Together with a moist soft paper, the sample was placed inside two plastic bags to prevent it from drying out. Even so, numerous salt crystals were seen on the surface of the plug when the sample was unwrapped ten years later, indicating drying which has caused, together with the low axial load, a few horizontal cracks (parallel to the bedding). Vertical cracks are also observed on SEM pictures (fig. 2). These cracks will be closed in the early phase of the test due to the application of a confining pressure, but may affect the permeability, breakthrough pressure and acoustic velocity when the pore pressure is increased during CO_2 injection into the sample.

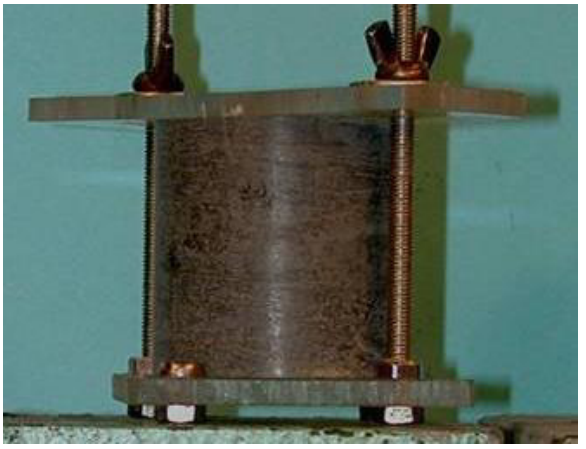

Figure 1: Fresh sample of Draupne shale (under moderate confinement) used in this study

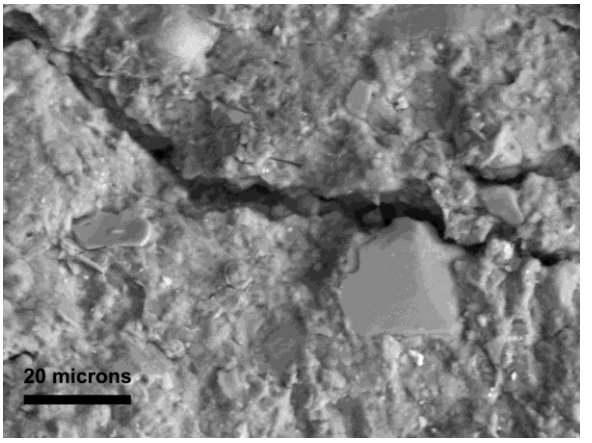

Figure 2: SEM picture of a vertical crack in the Draupne shale (the bedding is indicated by the clay minerals)

A few grams of the shale material were crushed to powder and examined using X-ray powder diffraction (XRD). It has been performed on both the bulk sample and on the clay fraction (< 2 μm), which was separated from the rest of the sample by gravity settling of particles in suspension. Different methods have also been used to identify the clay minerals, and also to distinguish between quartz, K-feldspar and plagioclase. Table 1 shows the mineral composition obtained by XRD. It should also be noted that the Draupne formation has an average level of total organic carbon (TOC) between 5 and 10 wt % [10,11]. This is an important property since organic carbon dissolves easily in contact with CO_2.

The porosity of the sample has been thoroughly studied through different methods. First, the imbibition method

gave a relatively high porosity of 35 % and a dry density of 1.79 g/cm^3. Then mercury intrusion porosimetry (MIP) has been used to characterize the pore size distribution of the shale sample (fig. 3). It measured a total porosity of 21.0 %. The resolution of the MIP prohibits the detection of pore diameters smaller than 6 nm and bigger than 800 µm. The 21.0 % porosity is therefore underestimated because only calculated based on pores with diameter in this range. The median pore diameter was found to be 27.5 nm corresponding to the typical space between the grains of clay material. The smaller voids identified (10 nm and less) usually corresponds to the inner porosity of clay minerals, micritic cement or organic matter. MIP also gives a bulk density of 2.01 g/cm^3, and an underestimated value of grain density of 2.55 g/cm^3. The permeability of the sample is measured from a constant head permeability test. The obtained value of 60 nD is in good agreement with the pores size of the shale [12].

The microstructural characterization has been completed by a helium pycnometry test: successive porous network fillings with helium showed a skeletal density of 2.63 g/cm^3. This value is more precise than the one obtained from mercury porosimetry because helium has access to smaller pores than mercury and water due to lower surface tension. This skeletal density value raises the porosity to 23.7%. The excessive value of 35% of porosity obtained by the water saturation method is attributed to the numerous horizontal cracks that were created by unloading during the coring and sampling process and from 10 years storage in the NGI warehouse (confirmed by salt efflorescences along the horizontal cracks when the sample has been taken out of the warehouse). The reason why they are not recorded by other methods is that the pieces tested by these last two methods were prepared to contain neither natural cracks nor cracks from drying, in order to only observe the original microstructural properties.

To sum up, the core sample of Draupne shale has a primary porosity of 23.7%, with a main family of pore with entry size of 27.5 nm, 21.0% of primary porosity between 6 nm and 800 µm, and an approximate 11% of secondary porosity from microcracks. During the first phase of test, the cracks are assumed to be closed by the confining pressure and the porosity of the shale is considered to be 23.7%.

Mineral	Weight percent	
quartz	35.7	
Kfelspar	2.5	
Plagioclase	1.6	
dolomite/ankerite	14.6	
Pyrite	6.1	
Smectite	14.6	
illite/muscovite	9.2	clay fraction:
Kaolinite	12.3	39.5
Chrlorite	3.4	

Table 1: Mineral composition of the shales obtained by XRD

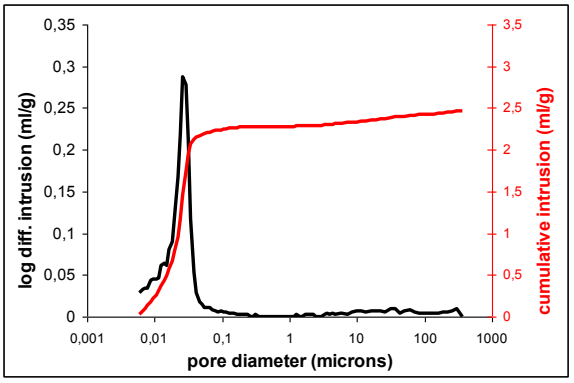

Figure 3: Pore entry diameter distribution in Draupne shale obtained from mercury intrusion porosimetry.

3. Methods

A special set up for flooding supercritical CO_2 through the Draupne shale sample has been developed (fig. 4). Fluids were to enter and exit the shale via two filters and two perforated plates to ensure an even distribution of fluid at the entry and the exit of the sample. The filters were connected to two syringe pumps. Two pressure sensors allowed the pore pressure in the sample to be constantly logged. One temperature sensor was set up close to each pressure sensor to have a constant control on the density of CO_2 in the device. The axial and radial strains of the sample were measured using Linear Variable Differential Transformers in axial and radial direction. The transit time of acoustic compressional waves (V_P) was measured using piezoelectric transducers. As both fluid viscosities and CO_2 solubility are closely related to temperature, efforts were made to keep the temperature constant. The cell and syringe pumps were therefore placed inside a *2*x*1*x*1* meter cabinet, which can withstand working temperatures up to 80ºC.

The capillary breakthrough pressure is a useful measure to quantify the ability of the caprock to prevent invasion

of CO_2 from the reservoir and into the overburden. In the literature [13] the breakthrough pressure of a rock sample corresponds to the injection pressure when the non-wetting phase first appears on the exit face of the sample. Here an estimation of the capillary breakthrough pressure for CO_2 in the Draupne shale is obtained from the Young-Laplace equation [14] $P_{cb} = 2\gamma \cos\theta / r$ by inserting the median pore radius (r), interfacial tension between brine and CO_2 (γ) and the wettability angle (θ) between CO_2, brine and host rock. The median pore radius for the Draupne shale is 13.5 nm, $\cos\theta$ can be expected between 0.9 and 0.75 [5] and interfacial tension is in the range 20 – 40 mN m^{-1} [15,16]. Inserting these values into the Young-Laplace equation gives a range of estimated breakthrough pressure between 2.2 and 5.3 MPa, with a mean value of 3.8 MPa.

The evaluation of the sealing capacity of this shale for CO_2 storage has been performed in two steps. After a thorough characterization of the sample, the first phase is a breakthrough test with supercritical CO_2. It consists, at a fixed confining pressure of 13 MPa, of increasing progressively the pore pressure gradient inside the cylindrical sample. A pore pressure of 7.5 MPa is kept fixed at the outlet face of the sample, while increasing the pore pressure at the inlet stepwise until a flow is observed. The pore pressure gradient for which steady state flow of CO_2 is first observed defines our "breakthrough pressure".

Finally the sample is left in the device with the obtained steady state flow for about 30 days. The aim of this "flow through test" is to simulate in the laboratory a long term contact between CO_2 (either dissolved in brine or in supercritical phase) and the Draupne shale, and check if any chemical reaction occurs (mainly dissolution or crystallization). The effects of the chemical reactions are evaluated afterwards by a petrophysical analysis (mercury intrusion porosimetry, helium pycnometry) of the tested shale sample.

4. Results

As stated earlier, several parameters have been continuously monitored during the test: the volume of fluids in the pumps, the axial and radial strain of the sample and the axial P-wave velocity. The entry volume decreases rapidly during the bottom pressure increase due to the high compressibility of CO_2 in these conditions. The main thing to notice is that it becomes linear during day 36 (fig. 5). The exit volume is stable until day 31, when it starts to increase progressively, reaching a linear increase approximately on day 58. The fluctuations of the pump volume of the exit pump after breakthrough is a result of temperature variations in the temperature chamber causing relatively large changes in fluid density due to presence of supercritical CO_2 and pressure conditions close to the critical point where the density of CO_2 is strongly temperature dependent. The radial and axial strains show different behavior during the test (fig. 6). Once again there is a significant change two days after the pressure gradient reaches 3.5 MPa on day 26: the sample is dilating in the radial direction while there is tiny compression in the axial direction. Notice that positive strain is defined as compression. The P-wave velocity remains constant in the first part of the test, until day 31 (fig. 7). Then, the P-wave velocity starts to slowly decrease until day 58 when it becomes more constant.

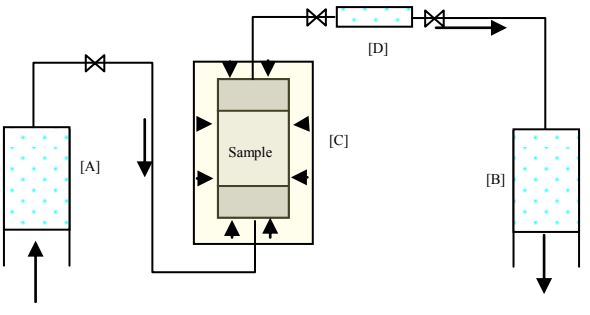

Figure 4: Experimental setup. [A] Entry pump compartment; [B] Exit pump compartment; [C] Rock sample under isotropic confinement; [D] Fluid sampling tube.

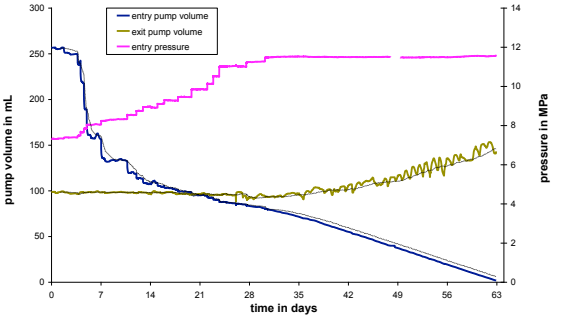

Figure 5: Temporal evolution of the fluid volumes in the entry and exit pumps (thin lines are sliding averages over 250 data points). Their evolution evaluates the amount of liquid flowing in and out of the sample. Entry pressure increase is added for time setting.

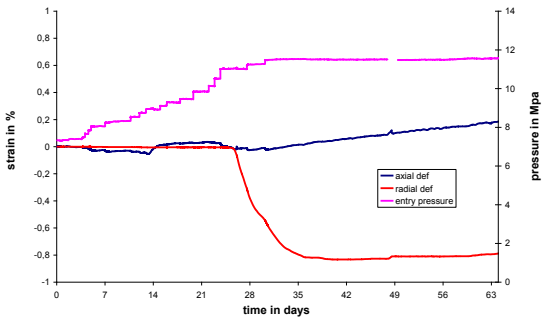

Figure 6: Temporal evolution of the axial and radial strain Entry pressure increase is added for time setting.

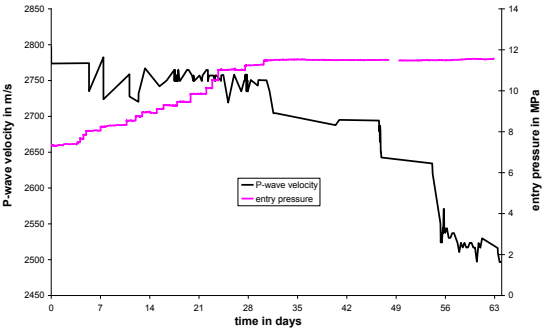

Figure 7: Temporal evolution of axial P-wave velocity. Entry pressure increase is added for time setting.

5. Discussion

5.1. Experimental model

From the experimental data it is possible to rebuild a model scenario of the experiment. It is divided into five steps depending on the variations described earlier (fig. 8):

1. Nothing happens when the pressure gradient is below 3.5 MPa (effective pressure above 2 MPa)
2. After two days (day 24 to 26) with a pressure gradient of 3.5 MPa (effective pressure of 2 MPa), the sample starts to dilate due to pore pressure increase (effective pressure decrease). It reveals that CO_2 starts to enter the sample from the bottom.
3. Five days later (day 31), the volume in the exit pump starts to increase indicating the breakthrough of CO_2 through the sample. This is confirmed by the simultaneous decrease of P-wave velocities. Again this has to be related with a pore pressure increase (effective pressure decrease) causing reopening of some cracks.
4. Five days later (day 36), the radial expansion ends exactly when the decrease of entry pump volume becomes linear. These are the consequences of filling of all the possible vertical pathways (cracks) through the sample and thus stabilizing the pore and effective pressure.
5. Finally, 23 days later (day 58), the decrease in P-wave velocities ends approximately when the exit pump volume increase starts to become linear. This suggests that the steady state flowthrough has been reached, the CO_2 having filled all the accessible room (mainly vertical and horizontal cracks) in the sample and the sample having reached its equilibrium.

The injection rate of CO_2 during the breakthrough process is very low. This implies that the capillary forces due to the CO_2-brine interfaces completely dominate the viscous forces in the fluids. Therefore, it is less likely that the obtained displacement pattern is dominated by so called viscous fingering; a process that results when a less viscous non-wetting fluid (here CO_2) is displacing at relatively high rate a more viscous wetting fluid (here brine) [17]. This is in good agreement with the model assessing that the flow pathways are directed mostly by cracks and also by some possible high permeable sections of the sample.

5.2. Post test sample and fluid analysis

In order to confirm the analysis obtained from the monitored data, several analyses have been performed on the sample once taken out of the cell. First, the tested sample has been weighed and measured and a new porosity of 30.2 % has been found. This value has to be considered cautiously because the sample was not regular and the

dimensions were not very constant. Some cracks have also been opened after removing the confining pressure. The final brine saturation of the samples varies then from 73 to 93 % depending on the chosen value of sample porosity. This brine saturation is very high suggesting only limited pathways of supercritical CO_2 through the sample.

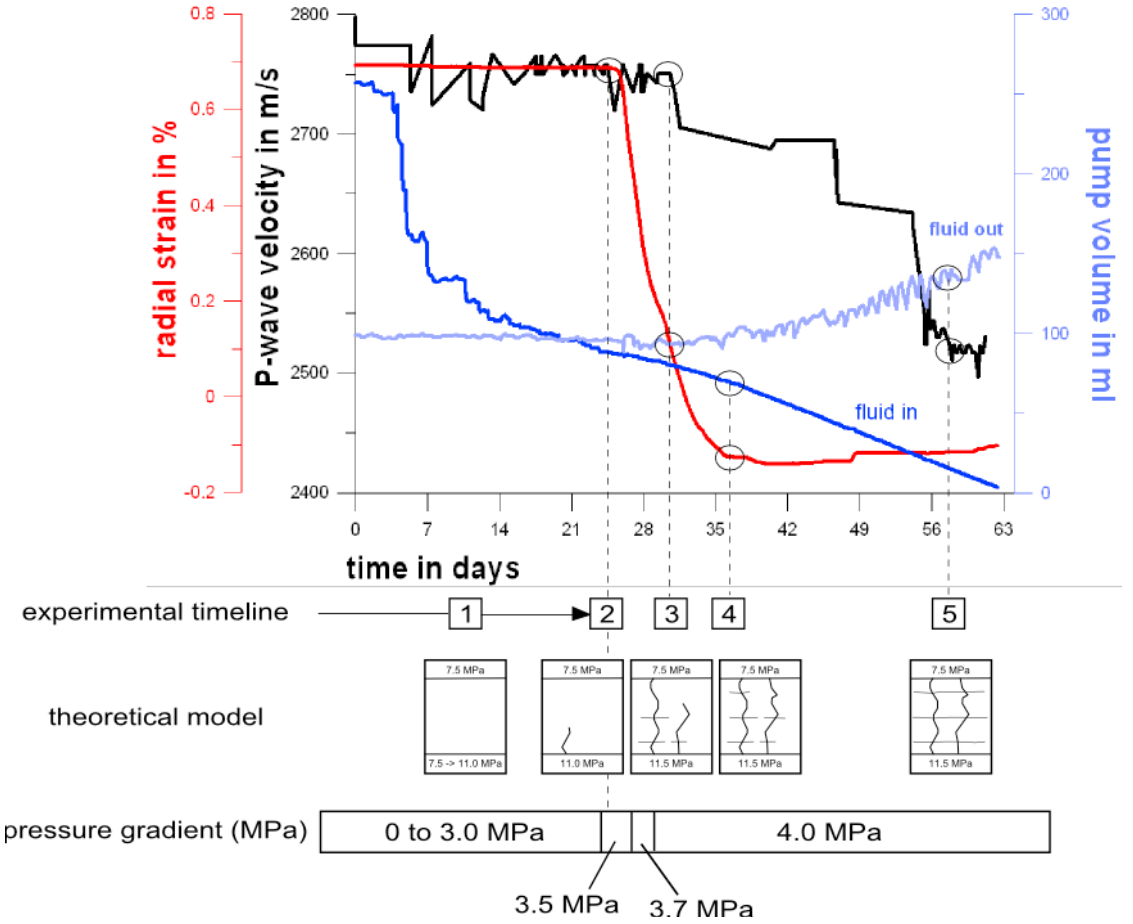

Figure 8: Analysis of correlation between data monitored during the test (the theoretical model shows the invasion of CO_2 in the sample)

The microstructural modifications of the Draupne shale during this test have been evaluated by MIP analysis performed on three parts extracted from the tested sample (fig. 9): one in the top, one in the middle and one in the bottom. The significant difference is that the bottom has been exposed to CO_2 on the whole surface during the whole test, as opposed to the top which has only been slightly exposed only after the breakthrough. This could obviously cause strong differences in the microstructural modifications of the sample (fig. 10).

The first thing to notice is that the three samples have common features: first, the main peak has a slightly lower volume associated to it. This is characteristic of the partial filling of the pores by halite crystals during drying [18], seen as white horizontal to sub-horizontal lines in the sample (fig. 10). The second common feature is that there is no significant change in the pores bigger than approximately 100 nm: no crack or dissolution has caused the apparition of a void bigger than this size. Nevertheless, there seem to be a significant difference in the smaller voids of the rock, smaller than 10 nm. The top and middle samples seem roughly similar to the original material (thus they are not represented on the figure to ease the reading), but the bottom sample shows fewer pores with entries of these small sizes. This porosity change could be associated with the dissolution of organic matter, which can enclose pores of these sizes: its dissolution implies a disappearance of these pores as can be seen on the spectra.

Finally, the sample of fluid flowing out of the shale contained a very high amount of gas. The weight of gas extracted at the exit of the sample was 7.3 g (15.5 ml) at 7.5 MPa and 35 degrees. Under STP this corresponds to a volume of 4.56 l. The extracted liquid was only weighing 0.47 g, corresponding to a volume of 0.46 ml (with a brine density of 1.0269 g/cm^3). Thus the tube contained 97.5 % (in volume) of gas and 2.5 % (in volume) of liquid. Gas chromatography on two samples of this gas showed a composition of 99 % of CO_2 and 1 % of H_2. This presence of H_2 could confirm the dissolution of organic matter during the test, but may also be caused by bacterial activity.

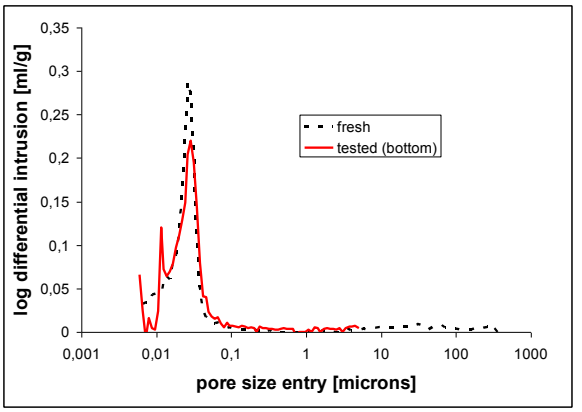

Figure 9: MIP spectra of the tested sample of Draupne compared to the fresh stone.

Figure 10: Sample of Draupen shale after CO_2 percolation

5.3. Comment on P-wave velocity variation

The measured reductions in P-wave velocity is expected because highly compressible supercritical CO_2 is replacing the less compressible brine inside the pores of the rock. At the pressure and temperature conditions of the experiment the compressibility and density of CO_2 is about 0.011 GPa and 0.254 g/cm^3 while brine has a compressibility and density of about 2 GPa and 1.03 g/cm^3. The Gassmann equation [19] is expressing the effect on the P-wave velocity due to fluid substitution in porous rock:

$$V_P^{\,2}\rho = \left(K_b + \frac{4}{3}\mu_b\right) + \frac{\left(1 - K_b / K_s\right)^2}{\left(1 - \phi - K_b / K_s\right)\frac{1}{K_s} + \frac{\phi}{K_f}}$$

where V_P denotes the P-wave velocity, ρ is the density, ϕ is the porosity, K_b and μb are the bulk and shear moduli of the porous rock frame, and K_s and K_f are the bulk moduli of the mineral matrix and the pore-filling fluid. By inserting typical values for shales like the Draupne shale we notice that 10% CO_2-saturation (90% brine saturation) could result in a P-wave reduction of about 13%. The reduction observed in our measurements is close to 10%. Dvorkin et al [20] have discussed the application of Gassmann equation to shaly sediments and have concluded that the Gassmann assumption may be violated in shale rich rock because the high amount of bonded water. However, a further study of this is beyond the scope of this paper.

The reduction in P-wave velocity could also be a result of re-opening of existing or creation of new fracture during the breakthrough process. The isotropic effective stress before CO_2 injection was 5.5 MPa. During the breakthrough process the effective stress at the entrance of the rock was reduced to 1.5 MPa creating an anisotropic stress regime that may result in local shear failure. In future studies more care should be taken to separate the effect of fluid invasion and fracture opening on the P-wave velocity.

6. Conclusion

This test on the Draupne formation sample allowed us to set up a method to evaluate the sealing efficiency of a caprock. The experiment was based on a breakthrough test of supercritical CO_2 into a brine saturated shale sample. The test was monitored with several geophysical measurements, which all agreed on the timing of the breakthrough: the increase of flow out correlated with a radial dilation of the sample and a reduction in the P-wave velocity. The results are strongly indicating flow of CO_2 along a few high permeable pathways due to re-opening of existing fractures. This evidence is supported by the strain measurements indicating radial dilation and fluid sampling showing that the exit fluid consisted of more than 96% pure CO_2 while the sample after the test contained a high amount of water. The measured breakthrough pressure ranging from 3.6 to 4.0 MPa is consistent with the theoretical estimation by the Young-Laplace law giving a range of breakthrough pressure from 2.2 – 5.3 MPa.

To sum up, the pore pressure increase at the bottom of the sample, simulating an accumulation of CO_2 in the reservoir caused a re-opening of the fractures in the lower part of the sample and started a flow along them. This flow through the cracks allowed a capillary percolation through the upper part of the sample where cracks are kept closed by the higher effective pressure. The experimental results indicate that re-activation of micro cracks in shale plays an important role for the percolation and flow of CO_2 in shale for the stress conditions given in the experiment.

7. Acknowledgements

This work was carried out at NGI under the project “Subsurface storage of CO_2 –, Risk Assessment, MOnitoring and REmediation” (SSC RAMORE). The project is founded by a consortium including The Research Council of Norway, StatoilHydro, RWE Dea, Norske Shell, Conocophillips and Schlumberger. Research performing partners are University of Oslo, University of Bergen, Insitute for Energy Research (IFE) and Norway Geotechnical Institute. Financial support is gracefully acknowledged.

The authors would also like to thank Gudmund Havstad and Sven Vangbæk for their great help in setting up the percolation cell and preparing the samples. Thanks to Ingar Johansen from IFE for performing the gas chromatography measurements. Thanks also to Fabrice Cuisiat and Lars Grande for the helpful discussions.

8. References

1. S. Schlömer and B.M. Krooss, Marine and Petroleum Geology 14 (1997) 563.
2. S. Li, M. Dong, Z. Li, S. Huang, H. Qing and E. Nickel, Geofluids 5 (2005) 326.
3. D.N. Dewhurst, R.M. Jones and M.D. Raven, Petroleum Geoscience 8 (2002) 371.
4. A. Busch, S. Alles, Y. Gensterblum, D. Prinz, D.N. Dewhurst, M.D. Raven, H. Stanjek and B.M. Kroos, International Journal of Greenhouse Gas Control 2 (2008) 297.
5. P. Chiquet, J.L. Daridon, D. Broseta and S. Thibeau, Energy Conversion and Management 48 (2007) 736.
6. T. Suekane, S. Soukawa, S. Iwatani, S. Tsushima and S. Hirai, Energy 30 (2005) 2370.
7. I. Gaus, M. Azaroual and I. Czernichowski-Lauriol, Chemical Geology 217 (2005) 319.
8. I. Okamoto, X.C. Li and T. Ohsumi, Energy 30 (2005) 2344.
9. J. Rutqvist, J.T. Birkholzer and C.F. Tsang, International Journal of Rock Mechanics & Mining Sciences 45 (2008) 132.
10. K. Knudsen, D. Leythaeuser, B. Dale, S. R. Larter and B. Dahl, Organic Geochemistry 13 (1988) 1051.
11. B. Dahl, Organic Geochemistry 35 (2004) 1551.
12. Y. Yang and A. Aplin, Journal of Geophsical Research 112 (2007) B03206
13. F.A.L. Dullen “Porous media: Fluid transport and pore structure” 2nd ed., Academic press, California, 1992
14. E.W. Washburn, Physical Review 17 (1921) 273.
15. S.J. Kemp, J. Pearce and E.J. Steadman, British Geological Survey Comissioned Report, CR/02/313. 2002.
16. B. Kvamme, T. Kuznetsova, A. Hebach, A. Oberhof and E. Lunde, Computational Materials Science 38 (2007) 506.
17. R. Lenormand, E. Touboul and C. Zarcone, Journal of Fluid Mechanics 189 (1988) 165.
18. M. Angeli, D. Benavente, J.P. Bigas, B. Menéndez, R. Hébert and C. David, Materials and Structures 41 (2008) 1091.
19. F. Gassmann, Vierteljahrsschrift der Naturforschenden Gesellschaft Zürich 96 (1951) 1.
20. J. Dvorkin, G. Mavko, and B. Gurevich, Geophysics 72 (2007) 1.